Chronic Colitis Exacerbates Nlrp3-dependent Neuroinflammation and Cognitive Impairment in Middle-aged Brain

Xiao-fei He
The third affiliated hospital of Sun Yet-Sun university
Li-li Li
The third affiliated hospital of Sun Yet-sun university
Wen-biao Xian
The First affiliated hospital of Sun Yet-sun university
Ming-yue Li
The third affiliated hospital of Sun Yet-Sun universiyu
Li-ying Zhang
The third affiliated hospital of Sun Yet-Sun university
Jing-hui Xu
The third affiliated hospital of Sun Yet-Sun university
Zhong Pei
The First affiliated hospital of Sun Yet-sun university
Hai-qing Zheng
The third affiliated hospital of Sun Yet-sun university
Xiquan Hu (huxiquan@mail.sysu.edu.cn)
The third affiliated hospital of Sun Yet-Sun university

Research

Keywords: Inflammatory bowel disease, Cognition, Glymphatic clearance, NLRP3 inflammasome, T cell

Posted Date: April 19th, 2021

DOI: https://doi.org/10.21203/rs.3.rs-414515/v1

Version of Record: A version of this preprint was published at Journal of Neuroinflammation on July 6th, 2021. See the published version at https://doi.org/10.1186/s12974-021-02199-8.

Abstract

Background: Neuroinflammation is a major driver of age-related brain degeneration and concomitant functional impairment. In patients with Alzheimer's disease, the most common form of age-related dementia, factors that enhance neuroinflammation may exacerbate disease progression, in part by impairing the glymphatic system responsible for clearance of pathogenic beta-amyloid. Inflammatory bowel diseases (IBDs) induce neuroinflammation and exacerbate cognitive impairment in the elderly. The NACHT-LRR and pyrin (PYD) domain-containing protein 3 (NLRP3) inflammasome have been implicated in neuroinflammation. We therefore examined if the NLRP3 inflammasome contributed to glymphatic dysfunction and cognitive impairment in an aging mouse model of IBD.

Methods: *Sixteen-month-old C57BL/6J and* NLRP3 *knockout* (KO) mice received 1% wt/vol dextran sodium sulfate (DSS) in drinking water to model IBD. The Morris water maze was used to examine spatial cognition, *in vivo* two-photon imaging to examine glymphatic clearance, and immunofluorescence staining and western blotting to detect markers of neuroinflammation.

Results: Administration of DSS induced colitis, impaired spatial cognition, activated microglia and increased A1-like astrocyte numbers. In addition, DSS treatment impaired glymphatic clearance, aggravated amyloid plaque accumulation, and induced neuronal loss in cortex and hippocampus. These neurodegenerative responses were associated with increased NLRP3 inflammasome expression and accumulation of gut-derived T lymphocytes along meningeal lymphatic vessels. Conversely NLRP3 depletion protected against cognitive dysfunction, neuroinflammation, and neurological damage induced by DSS.

Conclusions: Colitis can exacerbate age-related neuropathology, while suppression of NLRP3 inflammasome activity may protect against these deleterious effects of colitis.

Introduction

Neuroinflammation is strongly implicated in the pathogenesis of age-related cognitive decline, including that associated with Alzheimer's disease (AD), the most common form of dementia in older adults [1]. Patients with AD show progressive accumulation of misfolded amyloid-beta (Aβ) protein within plaques, and plaque load is directly associated with the severity of neurodegeneration and eventual functional deficits. However, some plaques may be observed 10–20 years before the onset of cognitive decline [2], so there is a substantial therapeutic window for curtailing disease progression Indeed, numerous strategies have been examined to reduce Aβ accumulation and prevent or slow down AD progression [2], but there are currently no widely effective treatments. Growing evidence indicates that accumulation of misfolded Aβ results from an imbalance between production and clearance [3], and that impairment of Aβ clearance is responsible for the most common type of AD [4] Thus, treatments that enhance Aβ clearance may be among the most broadly effective treatment strategies for AD.

The glymphatic pathway is a critical mechanism for amyloid beta clearance [5] and is markedly disrupted by neuroinflammation in aged brain [6, 7]. There is growing evidence for a regulatory role of the gut-brain axis in neuroinflammation and cognition. For example, inflammatory bowel diseases (IBDs) increase the incidence of cognitive impairment [8], while germ-free rearing and antibiotic treatment reduce cerebral Aβ pathology and neuroinflammation in AD model mice [9, 10]. Nevertheless, it is unclear if intestinal homeostasis regulates glymphatic function during the aging process.

Recent work has demonstrated that glymphatic clearance is dependent on meningeal lymphatic function [6]. However, it is unclear how meningeal lymphatic vessel function is regulated by the gut-brain axis in the elderly. The NACHT, LRR, and pyrin (PYD) domain-containing protein 3 (NLRP3) inflammasome are implicated in both gut immune homeostasis and neuroinflammation [11], and activation was found to exacerbate Aβ deposition and cognitive impairment in AD [12].

In the present study, we investigated possible contributions of the NLRP3 inflammasome to exacerbation of neurological dysfunction by colitis in aging mice. Oral administration of dextran sodium sulfate (DSS) for 4 weeks to model colitis increased NLRP3 inflammasome activity and gut-derived T cell numbers along meningeal lymphatic vessels (mLVs), activated microglia and astrocytes, impaired glymphatic clearance of Aβ, and aggravated cognitive decline, responses not found in NLRP3 knockout (KO) mice. Collectively, these results identified the NLRP3 inflammasome as a potential therapeutic target for AD and other neuroinflammatory disorders exacerbated by colitis.

Materials And Methods

Animals

The study was approved by the Animal Research Committee of Laboratory Animal Monitoring Institute of Guangdong Province (Guangzhou, China; committee's reference number: [2013]97). All efforts were made to minimize the number and suffering. NLPR3 KO mice were obtained from the Jackson laboratory (B6.129S6-Nlrp3tm1Bhk/J, Catalog number: 021302) and bred in the Laboratory Animal Monitoring Institute of Guangdong Province, they were founded on a C57BL/6J background. WT mice were provided from the Laboratory Animal Monitoring Institute of Guangdong Province. Male animals were used at sixteen months of age and were housed under a 12:12 h light: dark cycle (light on from 07:00 to 19:00 h), with controlled temperature and humidity. WT and NLRP3 KO mice were randomly divided into two groups: Control (Ctrl) and DSS group. In control group, mice received distilled water without DSS for 28 days. In DSS group, mice were treated with multiple-cycle administration of 1% wt/dextran sodium sulfate (DSS, (molecular weight 30,000 to 50,000, MP Biomedicals, CANADA) in drinking water on days 1 to 5, 8 to 12, 15 to 19, and 22 to 26, which was replaced by drinking water with fresh DSS solutions on day 6 to 7, 13 to 14, 20 to 21 and 27 to 28.

Open field

Wu used an open field arena to evaluate the anxiety and exploratory activities, which allowed the mice to freely explore for 5 min. The testing apparatus was a classic open field (a square arena, 50 × 50 cm, with walls 40 cm high), surmounted by a video camera. Each mouse was placed in the center of the arena, their performances were monitored and the time spent in the center (Region of interest, ROI) were recorded and analyzed.

Detection of lymphocytes migrated from the gut to the meninges

After finish of the DSS administration, we microinjected the fluorescent-cell-staining dyes CM-DiI (5μM in 2 μl of PBS per PP) (Life Technologies) cells in Peyer's patches (PPs) and paracolic nodes [13, 14].

Morris water maze task

Water maze tasks were performed after finish of the DSS administration as described previously (Fig. 1A) [15]. Briefly, mice received four trials (up to 60 s) on five consecutive training days, and then received a single 60 s probe trial on day 6. The latency to reach the platform during training days, the times crossing the target area (former platform position) and the time spent in the target quadrant during the probe trial were recorded.

In vivo two-photon imaging of glymphatic clearance

The efficiency of glymphatic clearance was evaluated using in vivo two-photon imaging [7]. Briefly, mice were anesthetized and a thin cranial window was created at parietal. Fluorescein isothiocyanate (FITC)-dextran (70 kDa; Sigma-Aldrich) was dissolved in artificial cerebrospinal fluid at a concentration of 1%, 10 μl of FITC was injected into the cisterna magna using a microsyringe connected with a syringe pump controller. 0.2 ml of 1% rhodamine B (Sigma) in saline was injected intravenously to show the brain vascular before imaging. Two-photon imaging was performed using a two-photon laser scanning microscope (Leica) equipped with a water immersion objective (25×). To monitor the clearance of FITC-dextran injected into the brain parenchyma, three-dimensional (3D) xyz stacks (512 × 512 pixels, 2 μm resolution) were taken up to 300 μm below the cortical surface at 5, 15, 30, 45, and 60 min after the injection of the FITC-dextran, the overall fluorescence intensities were analyzed. Besides, images 100 μm below the cortical surface were obtained and the fluorescence intensities in the paravascularv space were analyzed to examine the efficiency of glymphatic clearance.

Histology

Mice were perfused with 50 ml ice-cold phosphate buffer saline (PBS) and 50 ml of 4% (w/v) paraformaldehyde in PBS. For immunofluorescence staining, intact meninges were peeled off, and coronal brain slices 10 μm thick at interval of 100 μm or consecutive 40 μm were sectioned. Meninges or brain sections were boiled in citric acid buffer for 5 min in a microwave oven and were treated with 0.3% Triton X-100 and 10% goat serum for 1 h at room temperature and then incubated overnight at 4 ℃ with primary antibody [1:300 rabbit anti-ionized calcium binding adapter molecule 1 (Iba1) antibody, Wako,

Japan; 1:100 mouse anti-NLRP3 antibody, Thermo Fisher; 1:100 mouse purified anti-β-amyloid, 1–42 antibody, BioLegend; 1:100 mouse purified anti-β-amyloid, 1–40 antibody, BioLegend; 1:100 rabbit anti-CD31 antibody, Abcam; 1:300 rat anti-MAP2 antibody, Abcam; 1:300 mouse anti-GFAP, Sigma-Aldrich; 1:200 rabbit anti-AQP4, Peptide, USA; 1:100 rabbit anti-C3 antibody, Abcam; anti-NeuN, Millipore; 1:100 rabbit anti-LYVE1, Abcam] and then incubated with a secondary antibody [1:300 Anti-mouse IgG (H + L), $F(ab')_2$ Fragment (Alexa Fluor® 488 Conjugate); 1:300 Anti-rabbit IgG (H + L), $F(ab')_2$ Fragment (Alexa Fluor® 594 Conjugate), Cell signaling; 1:300 Anti-rat IgG (H + L), (Alexa Fluor® 488 Conjugate)] in PBS containing 10% normal goat serum at room temperature for 1 h.

Histological Scoring of Intestinal Inflammation

Body weight was monitored daily during the DSS administration, colitis model was confirmed by hematoxylin and eosin (H&E) staining and histological scorings were analyzed. Specifically, sections (2 cm) of the distal colon were cut, and then were sectioned (10-μm thick) at interval of 100μm using a frozen microtome (Leica, Germany). Colon sections were stained with hematoxylin and eosin (H&E) and histological scores were assessed as described by Xiao et al. and Chen et al. [16, 17].

Western blotting

For Western blotting, 30 μg protein in each lane was subjected to SDS-PAGE using 4–12% precast poly acrylamide gels (Novex, Invitrogen) at 200 V for 45 min. Then proteins were transferred to polyvinylidene fluoride membranes (Millipore, Bedford, MA, USA) at 120 V for 1.5 h. Membranes were incubated in 5% milk (R & D system) for 1 h and incubated with primary antibodies (mouse anti-NLRP3 antibody, Thermo Fisher; rabbit anti-IL-1beta antibody, Abcam; rabbit anti-caspase-1 antibody, Abcam; rabbit anti-Apoptosis associated speck (ASC), Affility, rabbit anti-tubulin beta antibody, Affinity) overnight at 4°C, followed by incubation with secondary antibody (anti-rabbit IgG, HRP-linked antibody, Cell Signaling Technology; anti-rat IgG, HRP-linked antibody, Cell Signaling Technology) for 1 h in a dark room. Images were obtained from a chemiluminescence imaging system.

Statistical Analyses

The 3D image overlays were visualized and analyzed with the Leica Application Suite (LAS) Advanced Fluorescence Lite software (LAS AF Lite, 2.4.1 build 6384, Leica). The ImageJ software (National Institutes of Health, Bethesda, MD, USA) was used to analyze the histological and western blotting results. For histological scoring of colon and NLRP3 expression, independent-samples t test was used to analyze. For other data, two-way repeated measures ANOVA with further turkey's multiple tests were used to analyze. A P value < 0.05 was considered statistically significant (Prism 8.0, GraphPad software, La Jolla, CA, USA). Data are expressed as means ± standard deviations of the means (SD).

Results

DSS administration induced colitis and activated the NLRP3 inflammasome in the brain.

We first compared histological signs of colitis, brain expression levels of the NLRP3 inflammasome, and accumulation of downstream proinflammatory factors between WT and NLRP3 KO mice under control conditions and following oral DSS administration for 4 weeks, then subjected groups of control and DSS-treated WT and NLRP3 KO mice to a battery of additional immunohistological and behavioral analyses (Fig. 1A). Oral DSS significantly enhanced expression of the NLRP3 inflammasome in wild type (WT) mice brains as evidenced by western blotting (Fig. 1B), while no NLRP3 expression was detectable in NLRP3 KO mice following DSS administration ($t = 1.167$, $P < 0.001$ vs. WTs by independent samples *t*-test) (Fig. 1B & C). Furthermore, two-way ANOVA revealed significant main effects of drug ($F = 32.62$, $P < 0.0001$) and genotype ($F = 26.20$, $P < 0.0001$) on expression of cleaved caspase-1, as well as a significant drug × genotype interaction ($F = 36.41$, $P < 0.0001$). Post hoc Tukey's tests further showed that DSS administration increased cleaved caspase-1 expression in WT mice ($P < 0.0001$) but not NLRP3 KO mice ($P > 0.05$), and post-DSS expression of cleaved caspase-1 was significantly lower in NLRP3 KO mice than DSS-treated WT mice ($P < 0.0001$) (Fig. 1B & C).

The NLRP3 inflammasome drove the inflammatory response in part by cleaving immature interleukin (IL)-1β to yield the active form, and ANOVA revealed significant main effects of drug ($F = 310.10$, $P < 0.0001$) and genotype ($F = 355.00$, $P < 0.0001$) on brain IL-1β expression as well as a significant drug × genotype interaction ($F = 608.80$, $P < 0.0001$) (Fig. 1D & E). In WT mice, brain expression of IL-1β was significantly greater following DSS treatment compared to WT controls ($P < 0.0001$), while no such change was detected in NLRP3 KO mice ($P > 0.05$), and expression was significantly lower in NLRP3 KO mice compared to WT mice following DSS ($P < 0.0001$). Similarly, there were significant main effects of drug ($F = 44.65$, $P < 0.0001$) and genotype on expression of the inflammasome adaptor protein ASC oligomer ($F = 45.47$, $P < 0.0001$) (Fig. 1F & G) as well as a significant drug × genotype interaction ($F = 66.36$, $P < 0.0001$). Expression of the ASC oligomer was significantly greater in DSS-treated WT mice compared to control WT mice ($P < 0.0001$), while there was no difference in expression between control and DSS-administered NLRP3 KO mice ($P > 0.05$), and expression was significantly lower in NLRP3 KO mice compared to WT mice following DSS ($P < 0.0001$). These results indicated that DSS administration activated the NLRP3 inflammasome in WT mice and increases the expression of the proinflammatory cytokine IL-1β.

NLRP3 depletion protected against colitis-induced neurological dysfunction.

Control and DSS-fed WT and NLRP3 KO mice were then compared for spontaneous behaviors and spatial cognition in the open field and Morris water maze tests, respectively. Time spent in the center of the open field, a behavioral index of anxiety, differed significantly among groups (Fig. 2A), with main effects of drug ($F = 18.88$, $P < 0.0001$) and genotype ($F = 14.28$, $P < 0.01$) as well as a significant drug × genotype interaction ($F = 16.57$, $P < 0.0001$). Post hoc analysis revealed a significant decrease in time spent in the central area among DSS-treated WT mice compared to control WT mice ($P < 0.0001$) but no such difference between DSS-administered and control NLRP3 KO mice ($P > 0.05$). Compared to DSS-fed WT mice, DSS-fed NLPR3 KO mice spent more time in the central area ($P < 0.001$).

Morris water maze performance also indicated significant cognitive dysfunction in DSS-fed WT mice but not in NLPR3 KO mice. During the training phase to find a hidden platform (Fig. 2B), there was a main effect of training day on latency as expected ($F = 62.39$, $P < 0.0001$), but no main effect of the group ($F = 2.20$, $P > 0.05$), training day × group interaction ($F = 0.93$, $P > 0.05$), or group differences within training days (all $P > 0.05$). However, in the probe trail for spatial memory in which the hidden platform was removed (Fig. 2C), there were significant main effects of the drug ($F = 6.27$, $P < 0.05$) and genotype ($F = 10.85$, $P < 0.01$) on the number of former platform location crossings and a significant drug × genotype interactions ($F = 6.26$, $P < 0.05$). Administration of DSS significantly reduced the number of former platform crossings among WT mice ($P < 0.01$) but not NLRP3 KO mice ($P > 0.05$), and the number of former platform location crossing was significant greater among DSS-fed NLRP3 KO mice than DSS-fed WT mice ($P < 0.01$)Similarly, there were significant main effects of drug ($F = 17.36$, $P < 0.001$) and genotype ($F = 15.83$, $P < 0.001$) on time spent in the target (former platform) quadrant and a significant drug × genotype interaction ($F = 11.08$, $P < 0.001$). Administration of DSS significantly reduced target quadrant time among WT mice compared to control WT mice ($P < 0.0001$) but had no effect on the performance of NLRP3 KO mice ($P > 0.05$), and DSS-fed NKRP3 KO mice spent more time in the target quadrant than DSS-fed WT mice *(*$P < 0.0001$). Collectively, these findings suggested that colitis induced a NLRP3 inflammasome-dependent spatial memory deficit. Next, we confirmed that the DSS administration induced colitis by H & E staining (Fig. 2D), the histological score was significantly decreased in NLRP3 KO mice compared with WT mice ($t = 2.46$, $P < 0.05$). Furthermore, the body weight of WT mice received DSS administration slightly decreased during the period of establishing the colitis model, whereas which was increased in other groups.

NLRP3 depletion inhibited colitis-induced microglial activation and protected against neuronal loss.

We then analyzed the effect of DSS on neuronal survival and the potential protection conferred by NLRP3 depletion (Fig. 3A-D). Consistent with the cognitive dysfunction induced by DSS in WT but not NLRP3 mice, there were main effects of the drug ($F = 13.68$, $P < 0.05$) and genotype ($F = 11.44$, $P < 0.05$) on neuron number in the cortex as well as a drug × genotype interaction ($F = 10.97$, $P < 0.05$). Furthermore, Tukey's tests showed that cortical neuron number was significantly lower in DSS-fed WT mice than control WT mice ($P < 0.05$) while there was no difference between DSS-fed and control NLRP3 KO mice ($P > 0.05$). The number of cortical neurons was greater in DSS-fed NLRP3 KO mice than DSS-fed WT group ($P < 0.05$) (Fig. 3A), suggesting the suppression of NLRP3 inflammasome activity protected against colitis-induced neuroinflammation and neurodegeneration. In hippocampus as well (Fig. 3B), there was a main effect of drug on neuronal number ($F = 8.43$, $P < 0.05$) but no significant main effect of genotype ($F = 4.86$, $P > 0.05$). Hippocampal neuron number was, however, significantly lower in DSS-fed WT mice than control WT mice ($P < 0.01$) but did not differ between DSS-fed and control NLRP3 KO mice ($P > 0.05$), and hippocampal neuron number was significant higher in DSS-fed NLRP3 KO mice than DSS-fed WT mice ($P < 0.05$). These results indicated that DSS administration induced neuronal loss in hippocampus, and that this neurodegenerative response was dependent on NLRP3.

We also quantified neuronal functional integrity by immunostaining for MAP2 in the cortex (Fig. 3C) and hippocampus (Fig. 3D). Two-way ANOVA revealed the significant main effects of drug ($F = 23.02$, $P < 0.01$) and genotype ($F = 29.29$, $P < 0.01$), as well as a significant drug × genotype interaction ($F = 100.30$, $P < 0.001$) on cortical MAP2 expression. Furthermore Tukey's multiple comparison test showed that mean MAP2 expression intensity was lower in cortex of DSS-fed WT mice than control WT mice ($P < 0.001$), but did not differ between control and DSS-fed NLRP3 KO mice ($P > 0.05$). Cortical MAP2 expression was also significantly higher in DSS-fed NLRP3 KO mice than DSS-fed WT mice ($P < 0.001$). In the hippocampus as well, two-way ANOVA revealed a significant main effect of drug ($F = 16.87$, $P < 0.01$) and genotype ($F = 66.06$, $P < 0.001$) on MAP2 expression intensity as well as a significant drug × genotype interaction ($F = 17.72$, $P < 0.01$). Post hoc Tukey's tests also indicated significantly lower MAP2 expression intensity in DSS-fed WT mice than control WT mice ($P < 0.01$) but no significant difference between DSS-fed and control NLRP3 KO mice ($P > 0.05$). Hippocampal MAP2 expression intensity was significant greater in DSS-fed NLRP3 KO mice than DSS-fed WT mice ($P < 0.01$).

NLRP3 depletion attenuated the colitis-induced amyloid beta deposition.

Among individuals destined to develop age-related mild cognitive impairment and AD, neuronal loss and neuroinflammation is associated with accumulation of Aβ, so we analyzed the effect of DSS administration on deposition of pathogenic Aβ (Aβ1–40, Aβ1–42) and the potential protective efficacy of NLRP3 depletion (Fig. 4). Consistent with cognitive and histological evaluations, two-way ANOVA showed significant main effects of drug ($F = 25.97$, $P < 0.01$) and genotype ($F = 15.66$, $P < 0.05$) on Aβ1–40 immunoexpression intensity as well as a significant drug × genotype interaction ($F = 134.00$, $P < 0.0001$) (Fig. 4A & B). Administration of DSS significantly increased Aβ1–40 expression in the cortex of WT mice ($P < 0.0001$) but not NLRP3 KO mice ($P > 0.05$), and cortical Aβ1–40 expression was significantly lower in DSS-fed NLRP3 KO mice then DSS-fed WT mice ($P < 0.0001$). In hippocampus as well (Fig. 4A & B), there was a main effect of drug on Aβ1–40 expression ($F = 5.63$, $P < 0.05$) but no main effect of genotype ($F = 18.00$, $P < 0.01$). There was, however, a significant drug × genotype interaction ($F = 7.03$, $P < 0.05$), and post hoc analyses indicated that DSS administration significantly increased Aβ1–40 deposition in the hippocampus of WT mice ($P < 0.05$) but not NLRP3 KO mice ($P > 0.05$), and that Aβ1–40 expression was significantly lower in DSS-fed NLRP3 KO mice than DSS-fed WT mice ($P < 0.05$) (Fig. 4A & B). Similarly, there were significant main effects of drug ($F = 56.97$, $P < 0.001$) and phenotype ($F = 29.92$, $P < 0.01$) on Aβ1–42 in the cortex (Fig. 4C & D) as well as a significant drug × genotype interaction ($F = 8.52$, $P < 0.05$). Administration of DSS also significantly increased Aβ1–42 deposition in the cortex of WT mice ($P < 0.05$) but not NLRP3 KO mice ($P > 0.05$), and Aβ1–42 expression was significantly lower in DSS-fed NLRP3 KO mice than DSS-fed WT mice ($P < 0.05$). Similarly, there were significant main effects of drug ($F = 71.24$, $P < 0.001$) and phenotype ($F = 9.95$, $P < 0.05$) on Aβ1–42 in hippocampus, and a significant drug × genotype ($F = 12.63$, $P < 0.05$). Furthermore, post hoc pair-wise comparisons revealed that DSS administration significantly increased hippocampal Aβ1–42 deposition in WT mice ($P < 0.01$) but not NLRP3 KO mice ($P > 0.05$), and that Aβ1–42 intensity was significantly lower in DSS-fed NLRP3 KO mice than DSS-fed WT mice ($P < 0.05$). Thus, colitis induced NLRP3-dependent Aβ accumulation in cortex and hippocampus,

possibly by suppressing glymphatic clearance, consistent with the observed neuropathology, neuroinflammation, and impaired spatial cognition.

NLRP3 depletion decreased astrocytic activation induced by colitis.

We then examined the effects of colitis and NLRP3 KO on astrocyte density and polarization of astrocytic AQP4 in cortex and hippocampus as measures of astrocytic activation and function. Two-way ANOVA analysis revealed significant main effects of drug ($F = 27.96$, $P < 0.0001$) and genotype ($F = 25.61$, $P < 0.0001$) on astrocyte density in cortex as well as a significant drug × genotype interaction ($F = 15.04$, $P < 0.001$) (Fig. 5A & B), while post hoc analyses revealed increased astrocyte density in DSS-fed WT mice compared to control WT mice ($P < 0.0001$) but no significant difference between DSS-fed and control NLRP3 KO mice ($P > 0.05$). Astrocyte density was significantly lower in DSS-fed NLRP3 KO mice compared to DSS-fed WT mice ($P < 0.0001$), suggesting that NLRP3 KO protected against neuroinflammation and reactive transformation of astrocytes.

There were no main effects of drug ($F = 0.40$, $P > 0.05$) or genotype on AQP4 expression ($F < 0.01$, $P > 0.05$) and no drug × genotype interaction ($F = 3.149$, $P > 0.05$) (Fig. 5A & B). There were also no significant pair-wise differences in AQP4 immunoexpression intensity among the four treatment groups (all $P > 0.05$) (Fig. 5A & B). Alternatively, there were significant main effects of drug ($F = 13.68$, $P < 0.01$) and genotype ($F = 11.45$, $P < 0.01$) on AQP4 distribution polarity in cortical astrocytes as well as a significant drug × genotype interaction ($F = 9.08$, $P < 0.01$) (Fig. 5A & B), and AQP4 polarity was significantly lower in DSS-fed WT mice than control WT mice ($P < 0.001$). Conversely, there was no difference in polarity between DSS-fed and control NLRP3 KO mice ($P > 0.05$) (Fig. 5A & B). Polarity was significantly higher in DSS-fed NLRP3 KO mice compared to DSS-fed WT mice ($P < 0.001$).

In the hippocampus as well (Fig. 5C & D), there were significant main effects of drug ($F = 28.40$, $P < 0.0001$) and genotype ($F = 20.48$, $P < 0.0001$) on astrocyte density, and a significant drug × genotype interaction ($F = 24.39$, $P < 0.0001$). According to post hoc analyses, astrocyte density was significantly higher in DSS-fed WT mice compared to control WT mice ($P < 0.0001$), but not significantly different between DSS-fed and control NLRP3 KO mice ($P > 0.05$). The density of hippocampal astrocytes was significantly lower in DSS-fed NLRP3 KO mice than DSS-fed WT mice ($P < 0.0001$).

As in the cortex, there was no main effect of drug ($F = 1.35$, $P > 0.05$) or genotype ($F = 0.87$, $P > 0.05$) on hippocampal AQP4 expression, nor a significant drug × genotype interaction ($F = 0.97$, $P > 0.05$). There were also no pair-wise differences in expression among the four groups (all $P > 0.05$). In contrast to the cortex, there was no main effect of genotype on AQP4 polarity ($F = 3.81$, $P > 0.05$), although there was a significant main effect of drug ($F = 9.12$, $P < 0.01$) and drug × genotype interaction ($F = 7.41$, $P < 0.05$). The polarity of AQP4 in hippocampus was also significantly lower in DSS-fed WT mice than control WT mice ($P < 0.001$) and did not differ between DSS-fed and control NLRP3 KO mice ($P > 0.05$). Polarity was significantly greater in DSS-fed NLRP3 KO mice compared to DSS-fed WT mice ($P < 0.05$). These findings suggested that DSS induced neuroinflammation and impaired astrocytic function through enhanced NLRP3 inflammasome activity.

NLRP3 depletion decreased the elevation in A1-like astrocyte numbers induced by colitis.

We investigated the effect of DSS administration on astrocyte phenotype by GAFP and C3 immunofluorescence staining (Fig. 6). There was no significant main effects of genotype on astrocytic C3 expression in cortex (F = 4.81, $P > 0.05$), but there was a significant main effect of drug (F = 44.06, $P < 0.01$) and a significant drug × genotype interaction (F = 14.48, $P < 0.05$). Administration of DSS significantly increased cortical C3 expression in WT mice ($P < 0.05$) but not NLRP3 KO mice ($P > 0.05$), and cortical C3 expression was significantly lower in DSS-fed NLRP3 KO mice than DSS-fed WT mice ($P < 0.05$). Similarly, there was no main effect of genotype on C3-positive astrocyte number in cortex (F = 4.22, $P > 0.05$), but there was a main effect of drug (F = 14.50, $P < 0.01$) and a significant drug × phenotype interaction (F = 14.48, $P < 0.05$). Administration of DSS increased C3-positive astrocyte numbers in the cortex of WT mice ($P < 0.001$) but not NLRP3 KO mice ($P > 0.05$), and C3-positive astrocyte number was significantly lower in the cortex of DSS-fed NLRP3 KO mice compared to DSS-fed WT mice ($P < 0.01$) (Fig. 6A & B).

In the hippocampus (Fig. 6C & D), there were significant main effects of drug (F = 12.21, $P < 0.05$) and genotype (F = 10.95, $P < 0.05$) on C3 expression, and a significant drug × genotype interaction (F = 10.29, $P < 0.05$). Hippocampal C3 expression was significantly higher in DSS-fed WT than control WT mice ($P < 0.05$) but did not differ between DSS-fed and control NLRP3 KO mice ($P > 0.05$). Hippocampal expression was also significantly lower in DSS-fed NLRP3 KO mice than DSS-fed WT mice ($P < 0.05$) (Fig. 6C & D). Consistent with C3 expression levels, there were significant main effects of drug (F = 89.34, $P < 0.001$) and genotype (F = 142.50, $P < 0.0001$) on hippocampal C3-positive astrocyte number, and a significant drug × genotype interaction (F = 85.07, $P < 0.001$). The number of C3-positive astrocytes in hippocampus was significantly higher in DSS-fed than control WT mice ($P < 0.001$) but did not differ between DSS-fed and control NLRP3 KO mice ($P > 0.05$). The number of C3-positive hippocampal astrocytes was also significantly lower in DSS-fed NLRP3 KO mice than DSS-fed WT mice ($P < 0.001$) (Fig. 6C & D). These results indicated that DSS administration promoted the A1-like transformation of astrocytes and that this effect was dependent on NLRP3 activation.

NLRP3 depletion rescued the impairment in glymphatic clearance induced by colitis.

To directly examine the effect of colitis on glymphatic function, we measured FITC-dextran clearance *in vivo* using two-photon imaging (Fig. 7). Following intracisternal injection, FITC tracer moved along the cerebral vasculature and entered the cortical parenchyma. Three-dimensional analysis revealed a progressive rise in FITC fluorescence intensity for 30 min before decreasing in WT control and both NLRP3 groups, while the tracer signal continued to increase for 60 min in DSS-fed WT mice, suggesting impaired glymphatic clearance. Two-way ANOVA and post hoc analysis showed no significant main effect of drug (F = 1.55, $P > 0.05$) or genotype (F = 0.95, $P > 0.05$) at 5 min after tracer injection, no drug × genotype interaction (F = 1.3450, $P > 0.05$), and no significant pair-wise differences among groups (all $P > 0.05$). At 60 min after tracer injection, however, there were significant main effects of drug (F = 14.61, $P < 0.01$) and genotype (F = 8.81, $P < 0.01$) on FITC intensity, and a significant drug × genotype interaction (F

= 35.98, $P < 0.0001$). Tracer fluorescence intensity was significantly greater in DSS-fed than control WT mice ($P < 0.001$) but did not differ between NLRP3 KO groups ($P > 0.05$), and signal intensity was significantly lower in DSS-fed NLRP3 KO mice compare to DSS-fed WT mice at 60 min ($P < 0.0001$).

To examine the efficiency of interstitial fluid flow, we then analyzed FITC-dextran movement in the paravascular space at 100 μm below the cortical surface (Fig. 7C & D). In DSS-fed WT mice, FITC signal intensity kept increasing from 5 to 45 min postinjection, and then gradually decreased, while all other group demonstrated decreases in signal intensity staring 5 min following injection. At 5 min following injection, there was no significant main effects of drug (F = 0.27, $P > 0.05$) or genotype (F = 0.30, $P > 0.05$) on paravascular FITC intensity, and no significant drug × genotype interaction (F = 1.61, $P > 0.05$). Further post hoc Tukey's test also indicated no significant differences in FITC intensity among the four groups at 5 min post-injection (all $P > 0.05$). At 60 min following FITC-dextran injection, however, there were significant main effects of drug (F = 6.68, $P < 0.05$) and genotype (F = 48.83, $P < 0.001$) as well as a significant drug × genotype interaction (F = 87.95, $P < 0.001$), and FITC intensity was significantly higher in DSS-fed WT mice than control WT mice ($P < 0.001$) but did not differ between NLRP3 KO groups ($P > 0.05$). Signal intensity was significantly lower in DSS-fed NLRP3 KO mice compared to DSS-fed WT mice ($P < 0.001$). Collectively, these results indicated that DSS-induced colitis and neural NLRP3 inflammasome activity impaired glymphatic clearance, while NLRP3 inflammasome suppression mitigated this effect.

NLRP3 depletion inhibited meningeal accumulation of gut-derived T cells.

A previous study reported that the neuroinflammation associated with colitis was enhanced by migration of activated γδ T cells from the gut to the meninges [18], so we examined if the differences in neuroinflammation and functional deficits among groups reflected meningeal gut-derived T cell accumulation (Fig. 8). There were significant main effects of drug (F = 156.3, $P < 0.0001$) and drug × genotype interaction (F = 129.0, $P < 0.0001$) on CD3-positive cells in mLVs (Fig. 8A & C), and a significantly greater number of CD3-positive cells in the mLVs of DSS-fed WT mice than control WT mice ($P < 0.0001$) but not in the mLVs of DSS-fed NLRP3 KO mice compared to control NLRP3 KO mice ($P > 0.05$). Meanwhile, there were significant main effects of drug (F = 150.60, $P < 0.0001$) and phenotype (F = 148.80, $P < 0.0001$) on CM-Dil-positive (gut-derived) cell number in mLVs, and a significantly greater number of CM-Dil-positive cells in the mLVs of DSS-fed WT mice than control WT mice ($P < 0.0001$) but not in the mLVs of DSS-fed NLRP3 KO mice compared to control NLRP3 KO mice ($P > 0.05$). Moreover, CM-Dil-positive cell number was significantly lower in the mLVs of DSS-fed NLRP3 KO mice compared to DSS-fed WT mice ($P < 0.0001$) (Fig. 8B & C), suggesting that recruitment of gut-derived lymphocytes to the meninges was dependent on NLRP3 inflammasome activity.Immuofluorescence staining for the lymphatic endothelial cell marker LYVE1 revealed the presence of lymphocytes distributed along mLVs (Fig. 8D), there was no obvious NLRP3 inflammasome activity in the meninges of NLRP3 KO mice, while DDS feeding significantly enhanced NLRP3 inflammasome activity in WT mice (t = 6.68, $P < 0.0001$), but there was no significant main effect of drug (F < 0.01, $P > 0.05$) or genotype (F < 0.15, $P > 0.05$), no drug ×

genotype interaction (F = 1.09, $P > 0.05$), and no difference in LYVE1 staining intensity among groups (all $P > 0.05$) (Fig. 8D & E).

Discussion

There is compelling evidence that the gut-brain axis (GBA) regulates the progression of neurodegenerative diseases, including AD [19, 20], and that intestinal lesions even decades before AD diagnosis may accelerate the underlying neuropathological processes [2]. Consistent with this notion that intestinal lesions can exacerbate early AD-like pathology, intestinal inflammation induced by DSS disrupted glymphatic clearance, increased Aβ deposition, triggered neuroinflammation, and even impaired spatial cognition among aging mice. Furthermore, these pathological effects were dependent on the NLRP3 inflammasome as all were suppressed by NLRP3 knockout, underscoring the therapeutic potential NLRP3 inflammasome blockade for early treatment of AD.

Microglial activation by the NLRP3 inflammasome may be a critical contributor to increased Aβ deposition. First, microglia are the resident macrophages and primary immune cells in the central nervous system responsible for the phagocytosis and clearance of Aβ [21] and NLRP3 activation was found to promote pro-inflammatory responses of microglia and dampen Aβ clearance [22–24]. Moreover, microglial activation induced A1-like astrocyte transition, resulting in a phenotype that can no longer promote neuronal survival or synaptogenesis [25, 26]. Consistent with these findings, DSS-induced colitis increased microglial activation and A1-like astrocyte numbers, and these responses were inhibited by NLRP3 depletion. In addition to possible loss of neurotrophic functions, astrocytes from DSS-fed WT mice demonstrated reduced AQP4 polarity, which is essential for glymphatic clearance efficacy [7]. Dysfunction of glymphatic clearance has been shown to enhance Aβ deposition [27], and indeed DSS-fed WT mice showed greater Aβ accumulation concomitant with reduced glymphatic clearance of a dextran tracer as well as multiple additional signs of glymphatic impairment such as loss of AQP4 polarity.

Accumulation of gut-derived T cells in mLVs is another potential contributor to age-related neuropathology and cognitive decline [18]. Meningeal LVs alter the accessibility of immune neuromodulators to the brain parenchyma, thereby potentially exacerbating inflammation [28]. In addition, CD4 + T cells in meanings were reported to enter the CSF [29], mediate microglial activation, and enhance local pro-inflammatory cytokine production [18, 30, 31]. Using *in vivo* CM-DiI cell tracing, we found that CD4 + T cells in the paracolic lymph nodes migrated to the meninges. Furthermore, brain cytokines have been demonstrated to promote T cell infiltration [14]. The reduced neuropathology observed in NLRP3 KO mice following DSS-induced colitis may have resulted from lower mature IL-1β production and ensuing infiltration of fewer gut-derived T cells.

Dysfunction of mLVs due to DSS treatment may also contribute to Aβ plaque accumulation [32]. However, LYVE1 staining indicated that meningeal lymphatic endothelial cells were unaffected by colitis or NLRP3 depletion. Indeed, mLVs express a unique transcriptional signature, and meningeal lymphatic endothelial

cells do not undergo expansion during inflammation [32, 33]. There is a limitation in this study, which will be explored in the future. We cannot exclude the possibility that the protection conferred by NLRP3 depletion was due to attenuation of inflammation from experimental colitis [34, 35], as depletion also decreased the histological colitis score.

Conclusion

Our results demonstrated that intestinal inflammation triggered neuroinflammation and decreased glymphatic clearance efficacy in aging mice, resulting in increased Aβ deposition and ultimately in neuronal death and cognitive impairment. We further demonstrated that these effects were mediated in part by migration of gut-derived CD4 + T cells and activation of the NLRP3 inflammasome. These mechanisms linking gut to brain inflammation are potential therapeutic targets for treatment of neurodegenerative diseases such as AD.

Abbreviations

IBDs: Inflammatory bowel diseases; NLRP3: NACHT-LRR and pyrin (PYD) domain-containing protein 3; DSS: dextran sodium sulfate; Aβ: amyloid-beta; AD: Alzheimer's disease; mLVs: meningeal lymphatic vessels; KO: Knock out; IL-1β: interleukin-1β; ASC: Apoptosis associated speck; MAP2: Microtubule associated protein 2; ANOVA: Analysis of Variance; AQP4: Aquaporin-4; GAFP: Glial fibrillary acidic protein; *Iba1:* Ionized calcium binding adapter molecule 1; FITC: fluorescein isothiocyanate; GBA: gut-brain axis; CSF: Cerebrospinal fluid

Declarations

Ethics approval and consent for publication

The study was approved by the Animal Research Committee of Laboratory Animal Monitoring Institute of Guangdong Province (Guangzhou, China; committee's reference number: [2013]97).

Availability of data and materials

All data generated or analysed during this study are included in this published article [and its supplementary information files].

Competing interests

The authors have declared that no competing interests exist.

Funding

This work was supported by grants from the National Natural Science Foundation of China (81902285, 81871847, 81672261, 81972151, 8157228, 81873751), Guangdong Basic and Applied Basic Research

Foundation (2019A1515011444, 2017A030313493, 2019A1515011106), the Science and Technology Planning Key Project of Guangzhou, China (201803010119), Guangzhou health and medical collaborative innovation major projects (201604020009), the Guangdong Provincial Key Laboratory for Diagnosis and Treatment of Major Neurological Diseases (2017B030314103), The Southern China International Cooperation Base for Early Intervention and Functional Rehabilitation of Neurological Diseases (2015B050501003) and Chinese postdoctoral science foundation (2019M663283, 2020T130742).

Authors' contributions

Xiao-fei He, Li-li Li, Wen-biao Xian , Ming-yue Li, Li-ying Zhang and Jing-hui Xu performed the experiments. Xiao-fei He and Li-li Li drafted the manuscript. Li-ying Zhang and Hai-qing Zheng revised the manuscript. Hai-qing Zheng and Xi-quan Hu conceived and designed the research, and edited and revised the manuscript.

Acknowledgement

We thank Neurology department in the First Affiliated Hospital of Sun Yat-sen University (Guangdong Provincial Engineering Center for Major Neurological Disease Treatment; Guangdong Provincial Translational Medicine Innovation Platform for Diagnosis and Treatment of Major Neurological Disease) for providing the experimental equipment and Guangdong Laboratory Animals Monitoring Institute for breeding the NLRP3 *Knockout* mice.

References

1. Heneka MT, Kummer MP, Latz E. Innate immune activation in neurodegenerative disease. [J] *Nat Rev Immunol*. 2014;14(7):463–77.
2. Sochocka M. Donskow-Łysoniewska K, Diniz BS, et al. The Gut Microbiome Alterations and Inflammation-Driven Pathogenesis of Alzheimer's Disease-a Critical Review[J] Mol Neurobiol, 2019, 3(56): 1841–51.
3. Hardy J, Selkoe DJ. The amyloid hypothesis of Alzheimer's disease: progress and problems on the road to therapeutics. [J] Science. 2002;297(5580):353–6.
4. Wildsmith KR, Holley M, Savage JC, et al. Evidence for impaired amyloid β clearance in Alzheimer's disease. [J] Alzheimers res ther. 2013;5(4):33.
5. Iliff JJ, Wang M, Liao Y, et al. A paravascular pathway facilitates CSF flow through the brain parenchyma and the clearance of interstitial solutes, including amyloid β. [J] Sci Transl Med. 2012;4(147):147ra111.
6. *Mesquita* SD, *Louveau* A, *Vaccari* A, et al Functional aspects of meningeal lymphatics in ageing and Alzheimer's disease. [J] Nature, 2018, 560(7717):185–191.

7. He XF, Liu DX, Zhang Q, et al. Voluntary Exercise Promotes Glymphatic Clearance of Amyloid Beta and Reduces the Activation of Astrocytes and Microglia in Aged Mice. [J] Front Mol Neurosci. 2017;10:144.
8. Bonaz BL, Bernstein CN. Brain-Gut Interactions in Inflammatory Bowel Disease. [J] Gastroenterology. 2013;144(1):36–49.
9. Smith PA. The tantalizing links between gut microbes and the brain. [J] Nature. 2015;526(7573):312–4.
10. Dodiya HB, Kuntz T, Shaik SM, et al. Sex-specific effects of microbiome perturbations on cerebral Aβ amyloidosis and microglia phenotypes. [J] J Exp Med. 2019;216(7):1542–60.
11. Pellegrini C, Antonioli L, Calderone V, et al. Microbiota-gut-brain axis in health and disease: Is NLRP3 inflammasome at the crossroads of microbiota-gut-brain communications? [J] Prog Neurobiol. 2020;191:101806.
12. Heneka MT, Kummer MP, Stutz A, et al. NLRP3 is activated in Alzheimer's disease and contributes to pathology in APP/PS1 mice. [J] Nature. 2013;493(7434):674–8.
13. Singh V, Roth S, Llovera G, et al. Microbiota Dysbiosis Controls the Neuroinflammatory Response after Stroke[Z]. United States: Society for Neuroscience, 2016: 36, 7428–7440.
14. Feng Y, He X, Luo S, et al. Chronic colitis induces meninges traffic of gut-derived T cells, unbalances M1 and M2 microglia/macrophage and increases ischemic brain injury in mice. [J] Brain Res. 2019;1707:8–17.
15. He XF, Lan Y, Zhang Q, et al. Deferoxamine inhibits microglial activation, attenuates blood–brain barrier disruption, rescues dendritic damage, and improves spatial memory in a mouse model of microhemorrhages[J]. J Neurochem. 2016;138(3):436–47.
16. Xiao H, Lin C, Ho DHH, et al. Inhibitory Effect of the Gallotannin Corilagin on Dextran Sulfate Sodium-Induced Murine Ulcerative Colitis[J]. J Nat Prod. 2013;76(11):2120–5.
17. Chen J, Jayachandran M, Zhang W, et al. Dietary Supplementation with Sea Bass (Lateolabrax maculatus) Ameliorates Ulcerative Colitis and Inflammation in Macrophages through Inhibiting Toll-Like Receptor 4-Linked Pathways[J]. Int J Mol Sci. 2019;20(12):2907.
18. Benakis C, Brea D, Caballero S, et al. Commensal microbiota affects ischemic stroke outcome by regulating intestinal gammadelta T cells. [J] Nat Med. 2016;22(5):516–23.
19. Ambrosini YM, Borcherding D, Kanthasamy A, et al. The Gut-Brain Axis in Neurodegenerative Diseases and Relevance of the Canine Model: A Review. [J] Front Aging Neurosci. 2019;11:130.
20. Zhang T, Han Y, Wang JY, et al. Comparative Epidemiological Investigation of Alzheimer's Disease and Colorectal Cancer: The Possible Role of Gastrointestinal Conditions in the Pathogenesis of AD. [J] Front Aging Neurosci, 2018(10): 176.
21. Datta M, Staszewski O, Raschi E, et al. Histone Deacetylases 1 and 2 Regulate Microglia Function during Development, Homeostasis, and Neurodegeneration in a Context-Dependent Manner. [J] Immunity. 2018;48(3):514–29.

22. Liu S, Liu Y, Hao W, et al. TLR2 is a primary receptor for Alzheimer's amyloid beta peptide to trigger neuroinflammatory activation [J]. J Immunol. 2012;188(3):1098–107.
23. Montacute R, Foley K, Forman R, et al. Enhanced susceptibility of triple transgenic Alzheimer's disease (3xTg-AD) mice to acute infection.[J]. J Neuroinflammation. 2017;14(1):50.
24. Lin C, Zhao S, Zhu Y, et al. Microbiota-gut-brain axis and toll-like receptors in Alzheimer's disease [J]. Comput Struct Biotechnol J. 2019;17:1309–17.
25. Liddelow S, Guttenplan K, Clarke L, et al. Neurotoxic reactive astrocytes are induced by activated microglia. [J] Nature. 2017;7638(541):481–7.
26. Clarke LE, Liddelow SA, Chakraborty C, et al. Normal aging induces A1-like astrocyte reactivity. [J] Proc Natl Acad Sci U S A. 2018;115(8):E1896–905.
27. Zhang Y, Huang R, Cheng M, et al. Gut microbiota from NLRP3-deficient mice ameliorates depressive-like behaviors by regulating astrocyte dysfunction via circHIPK2. [J] Microbiome. 2019;7(1):116.
28. Mesquita SD, Fu Z, Kipnis J. The Meningeal Lymphatic System: A New Player in Neurophysiology.[J] Neuron, 2018, 100(2): 375–388.
29. Schlager C, Korner H, Krueger M, et al. Effector T-cell trafficking between the leptomeninges and the cerebrospinal fluid. [J] Nature. 2016;530(7590):349–53.
30. Zhao H, Wan L, Chen Y, et al. FasL incapacitation alleviates CD4 + T cells-induced brain injury through remodeling of microglia polarization in mouse ischemic stroke. [J] J Neuroimmunol. 2018;318:36–44.
31. Buckwalter MS, Coleman BS, Buttini M, et al. Increased T Cell Recruitment to the CNS after Amyloid β1–42 Immunization in Alzheimer's Mice Overproducing Transforming Growth Factor-β1. [J] J Neurosci. 2006;26(44):11437–41.
32. Louveau A, Herz J, Alme MN, et al. CNS lymphatic drainage and neuroinflammation are regulated by meningeal lymphatic vasculature. [J] Nat Neurosci. 2018;21(10):1380–91.
33. Ahn JH, Cho H, Kim JH, et al. Meningeal lymphatic vessels at the skull base drain cerebrospinal fluid. [J] Nature. 2019;572(7767):62–6.
34. Umiker B, Lee HH, Cope J, et al. The NLRP3 inflammasome mediates DSS-induced intestinal inflammation in Nod2 knockout mice. [J] Innate Immun. 2019;25(2):132–43.
35. Yao X, Zhang C, Xing Y, et al. Remodelling of the gut microbiota by hyperactive NLRP3 induces regulatory T cells to maintain homeostasis. [J] Nat Commun. 2017;8(1):1896.

Figures

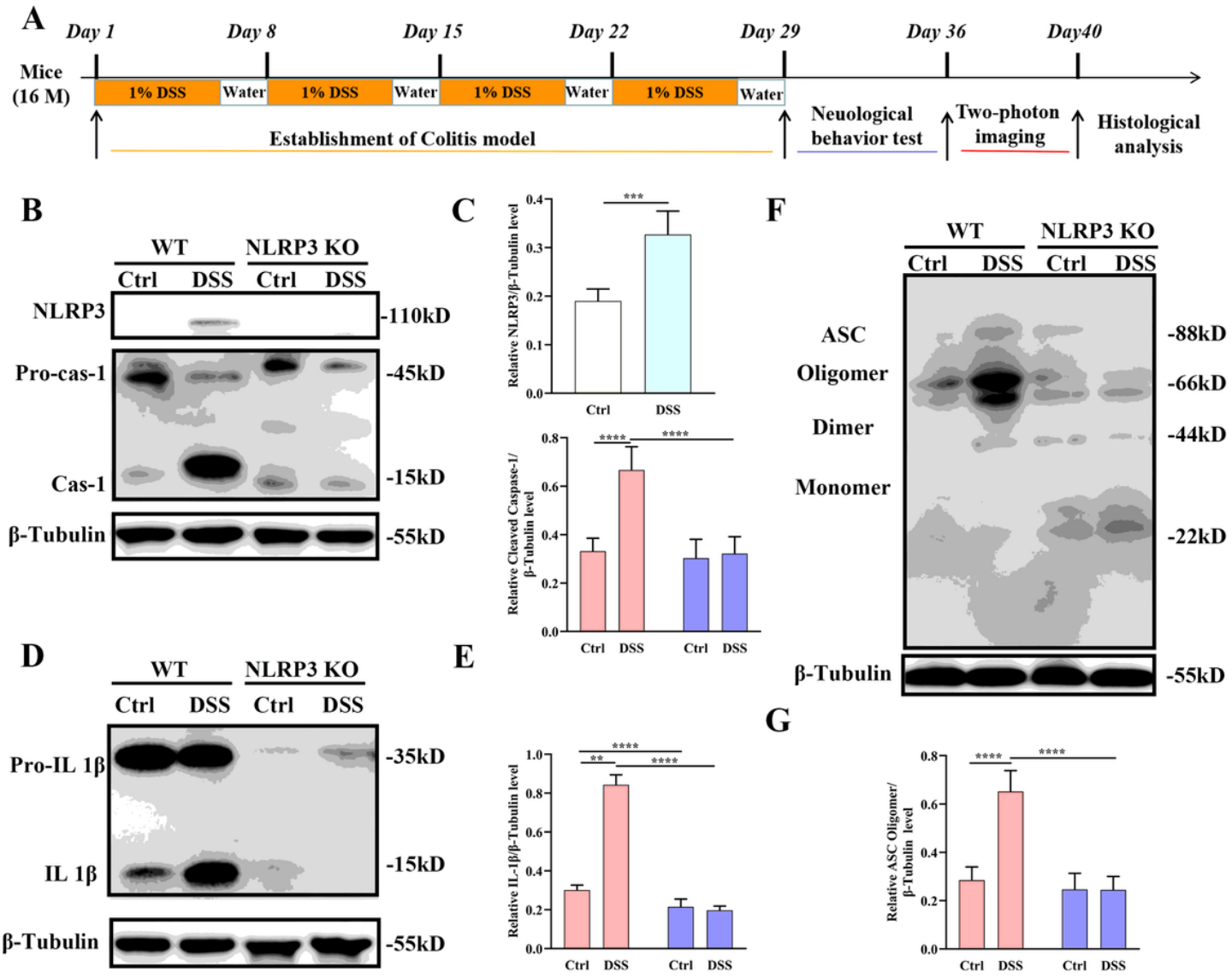

Figure 1

Induction of colitis by addition of dextran sodium sulfate (DSS) to drinking water (1% vol/vol) for 4 weeks induced the Colitis and increased NLRP3 activation in the brain of WT mice. A. Schematic diagram of the experimental design. B. Chemiluminescence imaging of NLRP3, caspase-1, and β-tubulin immunoexpression on western blots. C. Comparisons of NLRP3/β-tubulin and cleaved caspase 1/β-tubulin ratios among control WT, DSS-fed WT, control NLRP3 KO, and DSS-fed NLRP3 KO mice. D. Chemiluminescence image of IL-1β and β-tubulin immunoexpression by western blot. E. Comparisons of IL-1β/β-tubulin among treatment groups. F. Chemiluminescence image of ASC and β-tubulin immunoexpression by western blot. G. Comparisons of ASC oligomer/β-tubulin among treatment groups.

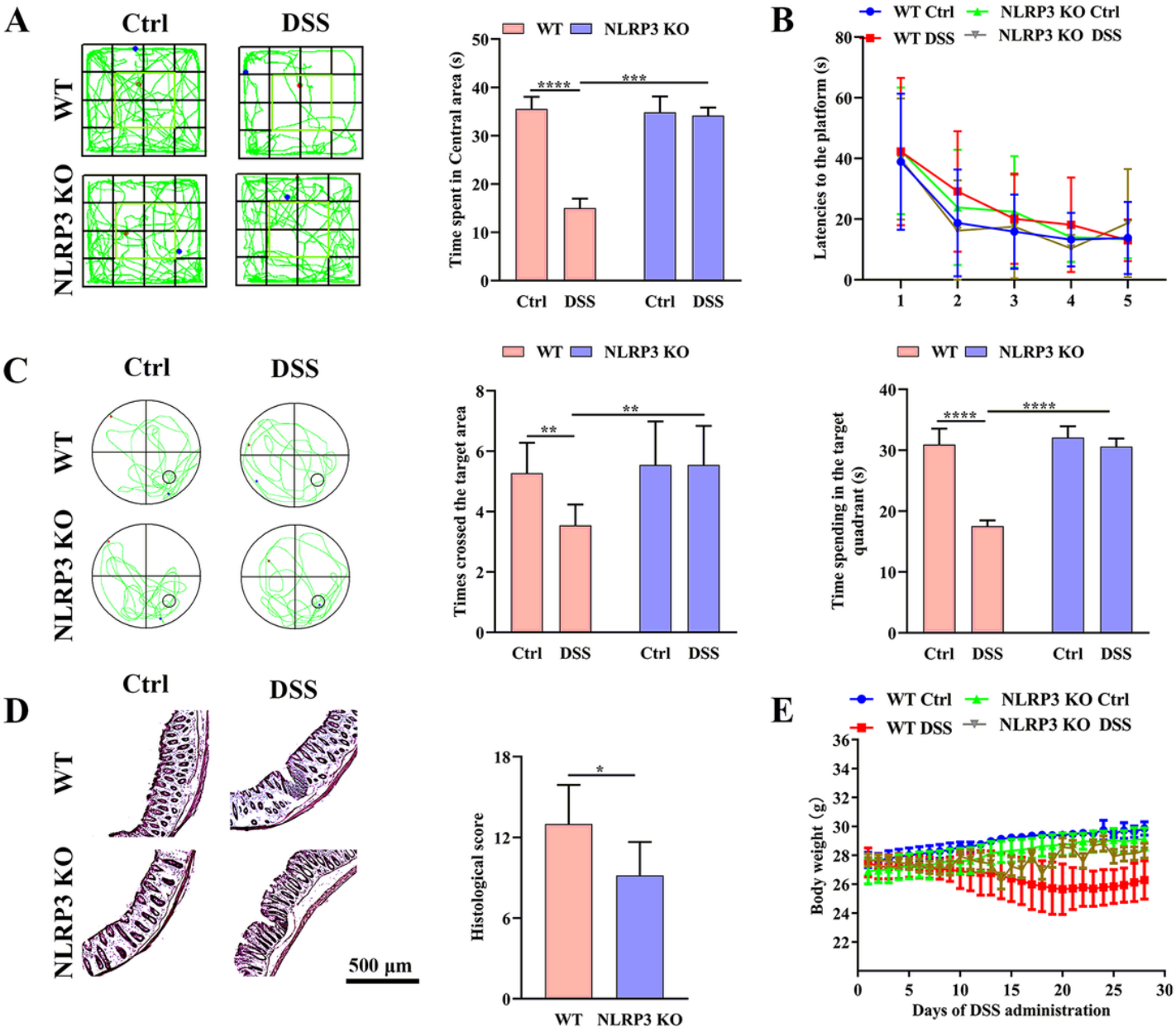

Figure 2

Induction of colitis by addition of dextran sodium sulfate (DSS) to drinking water (1% vol/vol) for 4 weeks altered spontaneous motor behavior and impaired spatial memory in aged (16-month-old) wild type (WT) mice but not age-matched NLRP3 KO mice. A. Representative movement tracks in the open field test showing less time spent in the central area by DSS-fed WT mice compared to untreated control (Ctrl) WT mice but no difference between DSS-fed and control NLRP3 KO mice. B. Latencies to the platform during the 5 days of Morris water maze training. C. Representative swim paths during the probe trial for spatial memory showing that DSS-fed WT mice made fewer crossings over the former platform location and spent less swim time in the target quadrant than control WT mice, indicating spatial memory impairment, while these values did not differ between DSS-fed and control NLRP3 KO mice. D. Hematoxylin and eosin (H & E) staining of the colon and comparison of histological scores among WT, DSS-fed WT, NLRP3 KO,

and DSS-fed NLRP3 KO mice. E. The line diagram shows the changes in body weight during the establishment of colitis.

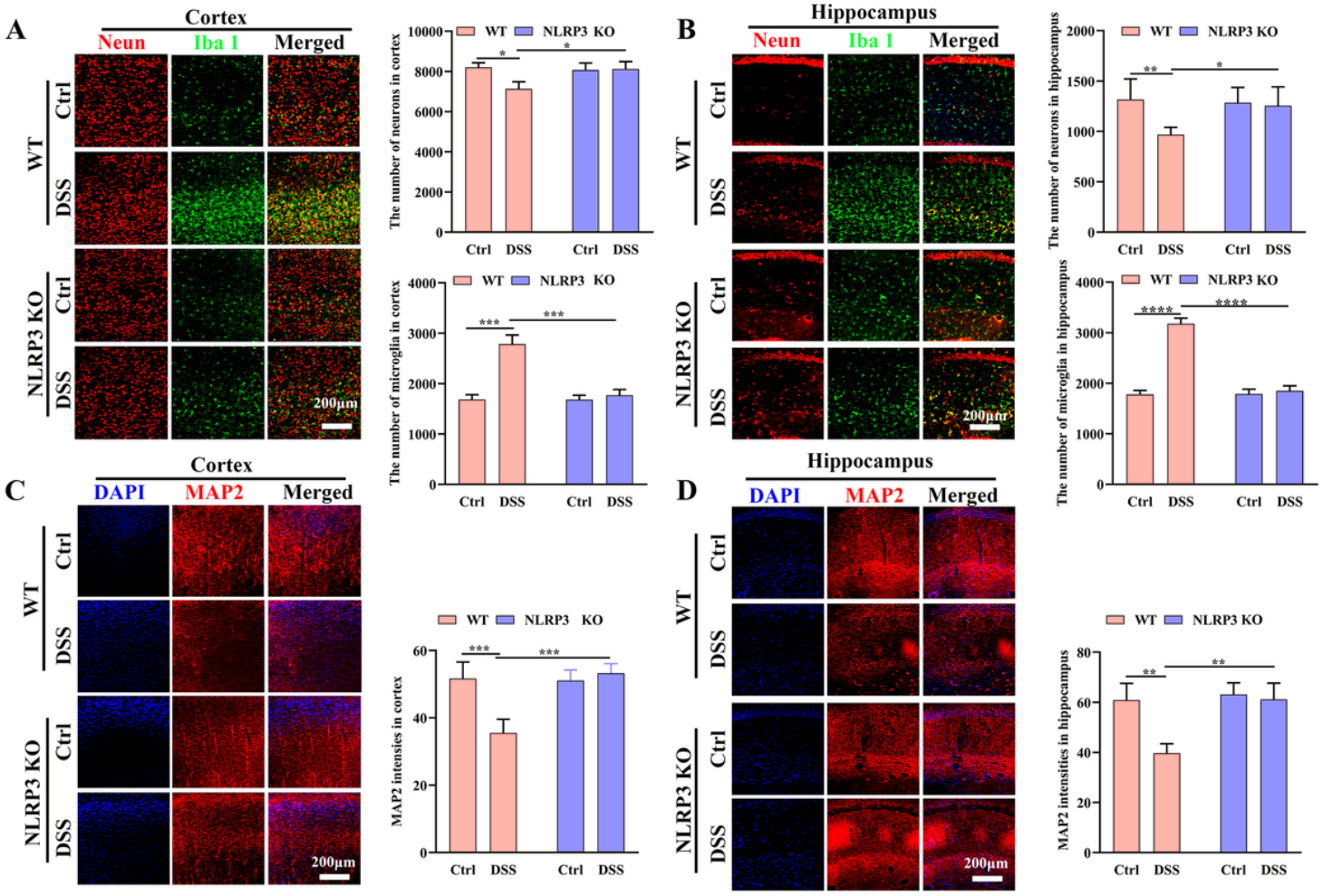

Figure 3

NLPR3 knockout protected against neuroinflammation and neurodegeneration from DSS administration. A. Immunofluorescence staining and comparison of neurons and microglia in cortex (25× water immersion objective) among control WT, DSS-fed WT, NLRP3 KO, and DSS-fed NLRP3 KO mice (average of four fields/slice, five slices per mouse, 6 mice per group). B. Immunofluorescence staining and comparison of neurons and microglia in hippocampus (CA1 area, 25× water immersion objective) among treatment groups (CA1 area, average of two fields/slice, five slices per mouse, 6 mice per group). C. Immunofluorescence staining of MAP2 (25× water immersion objective) and omparison of MAP2 staining intensities in cortex among treatment groups (average of four fields/slice, five slices per mouse, 6 mice per group). G. Immunofluorescence staining of MAP2 in hippocampus (CA1 area, 25× water immersion objective) and comparison of MAP2 staining intensities in hippocampus among treatment groups (average four fields/slice, five slices per mouse, 6 mice per group).

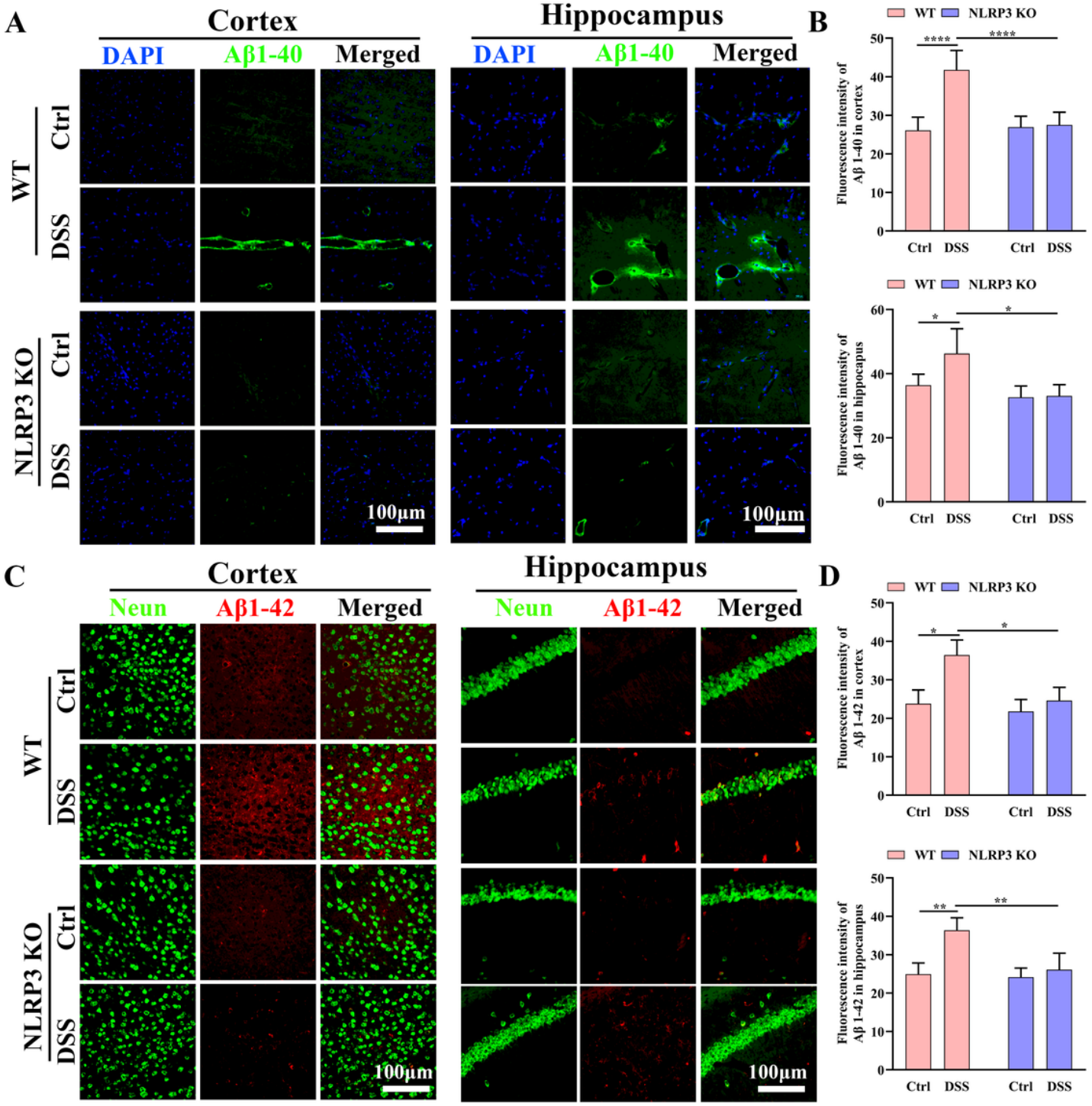

Figure 4

Colitis increased Aβ accumulation in WT mice but not NLRP3 KO mice. A. Representative images of Aβ1-40 fragment immunoexpression in cortex and hippocampus (40× objective). B. Comparison of Aβ1-40 expression intensity in cortex and hippocampus among control WT, DSS-fed WT, NLRP3 KO mice and DSS-fed NLRP3 KO mice. C. Representative images of Aβ1-42 fragment immunoexpression and neurons in cortex and hippocampus (40× objective). D. Comparison of Aβ1-42 expression intensity in cortex and hippocampus among treatment groups.

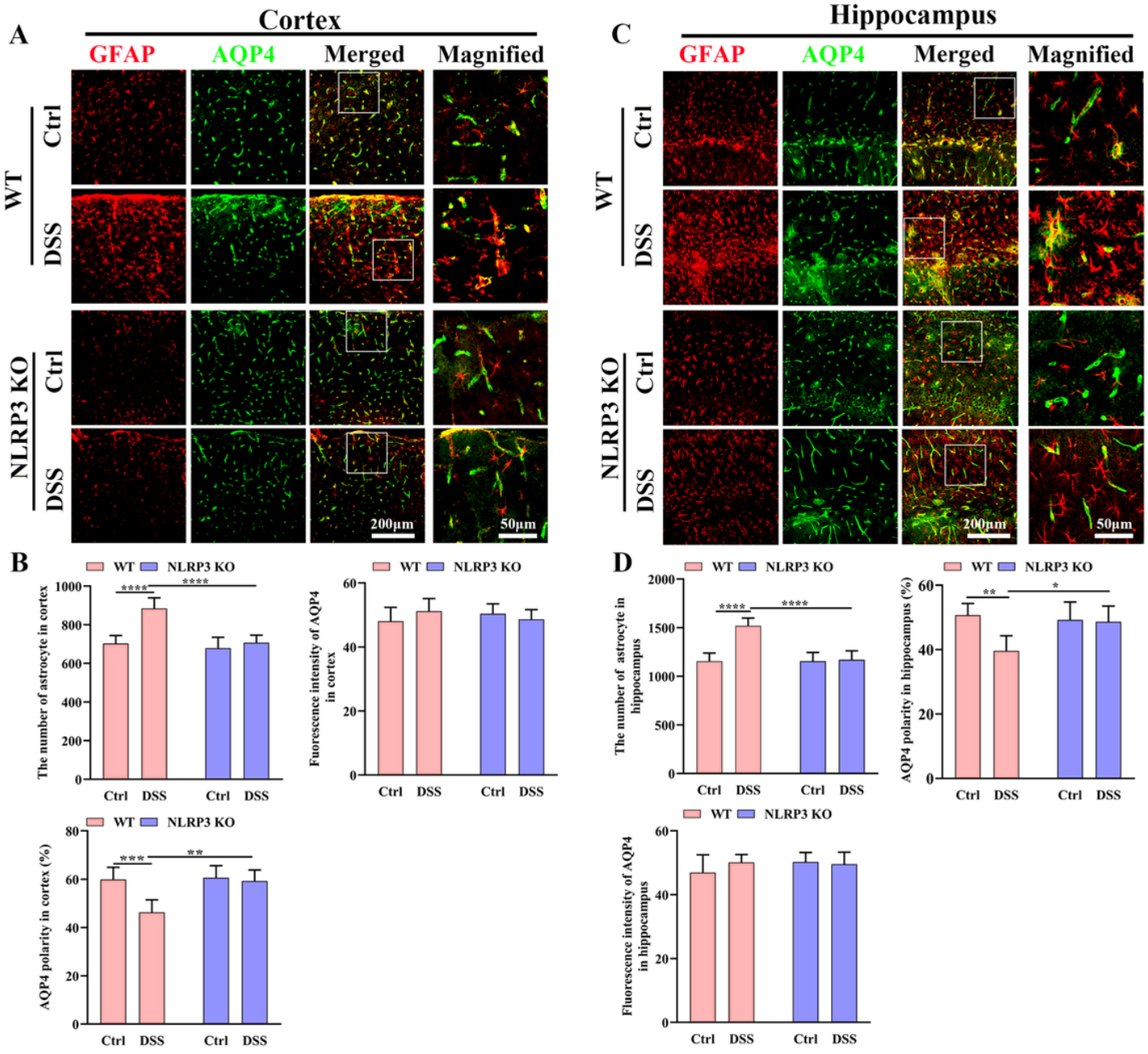

Figure 5

Colitis disrupted the polarity of astrocytic AQP4 distribution in WT but not NLRP3 KO mice. A. Representative images of astrocytes and AQP4 expression in cortex (Left 3 rows: 25× water immersion objective; right row: expanded images (3×) of regions in the white boxes). B. Comparison astrocyte number, AQP4 expression intensity, and AQP4 polarity in cortex among control WT, DSS-fed WT, NLRP3 KO, and DSS-fed NLRP3 KO mice. C. Representative images of astrocytes and AQP4 expression in hippocampus (Left three rows: 25× water immersion objective; right row: expanded images (3×) of regions in the white boxes). D. Comparison of astrocyte number, AQP4 expression intensity, and AQP4 polarity in hippocampus among treatment groups. Each dataset is expressed as mean ± SD.

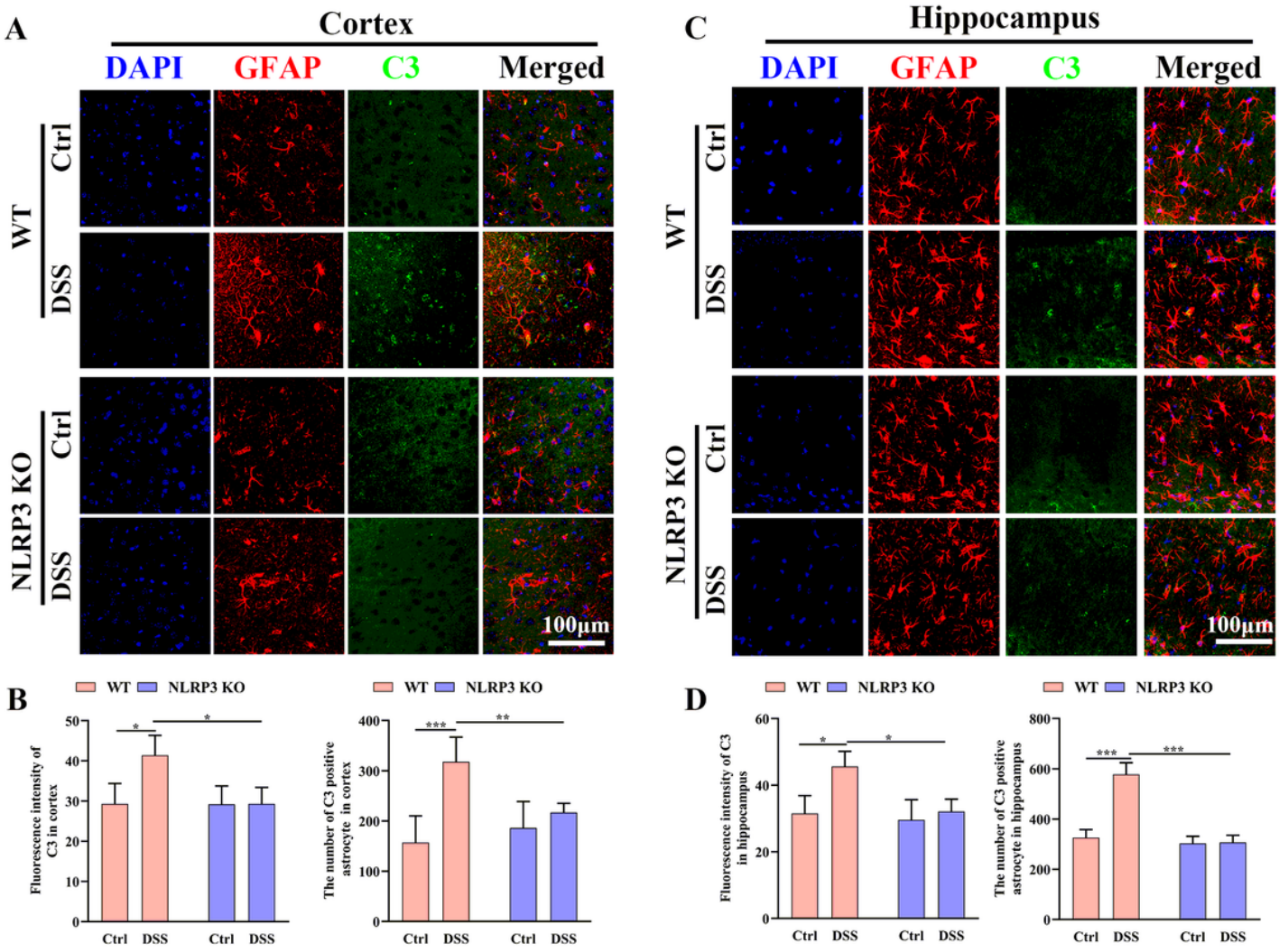

Figure 6

Colitis promoted transformation to the A1-like astrocyte phenotype in WT mice but not NLRP3 KO mice. A. Representative images of C3 immunoexpression and astrocyte in cortex (63× oil immersion objective). B. Comparison of C3-positive (A1-like) astrocyte number in cortex among control WT, DSS-fed WT, NLRP3 KO, and DSS-fed NLRP3 KO mice. C. Representative images of C3 immunoexpression and astrocytes in hippocampus (63× oil immersion objective). D. Comparison of C3-positive (A1-like) astrocyte number in hippocampus among treatment groups.

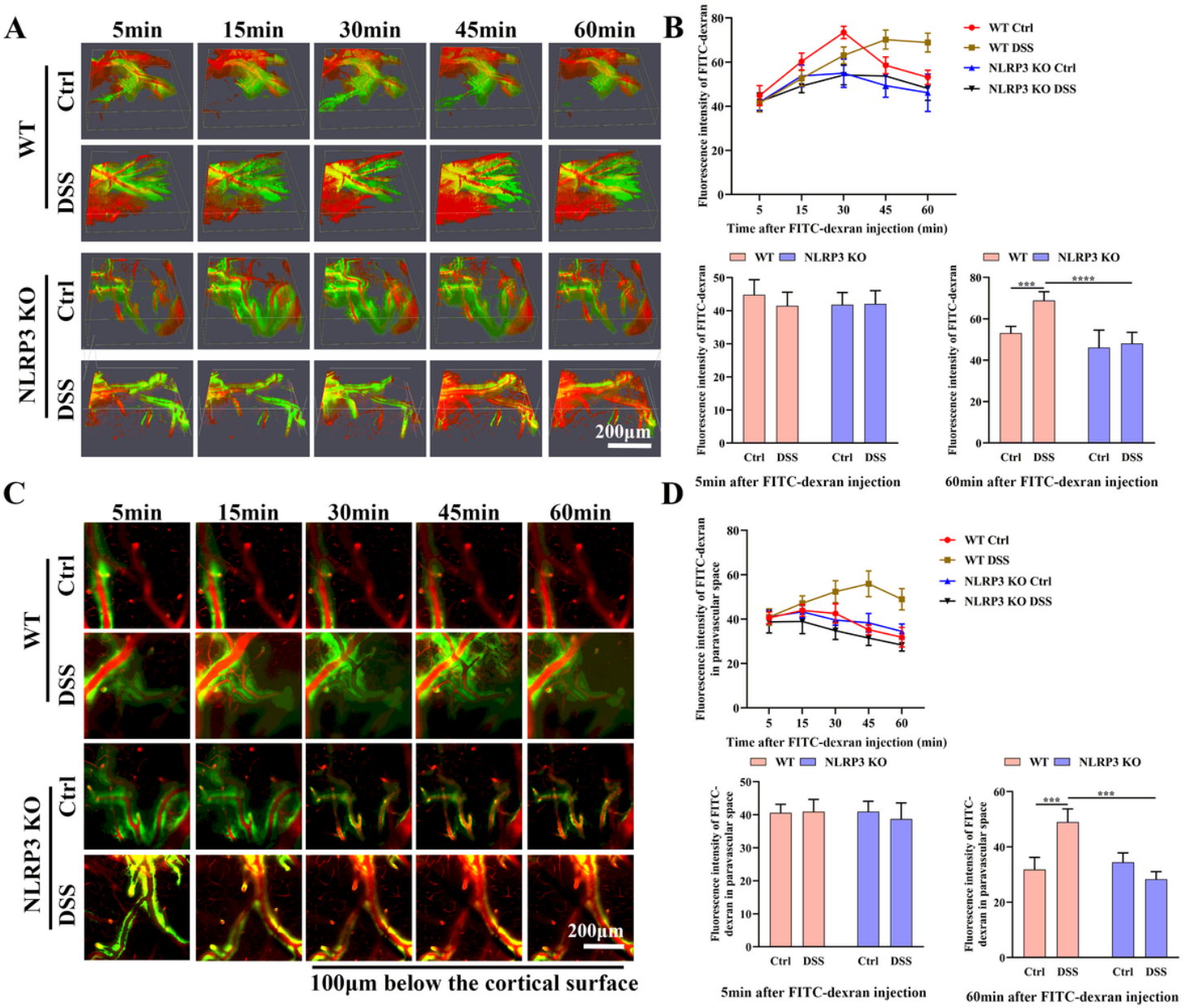

Figure 7

Colitis impaired the glymphatic clearance in WT mice but not NLRP3 KO mice. A. Representative images of three-dimensional images at 5min, 15min, 30min, 45min and 60min after infusion of FITC-dextran in cisterna magna (25× water immersion objective). B. Linear and histogram analysis of overall FITC-detran intensity at different time points after infusion among control WT, DSS-fed WT, control NLRP3 KO mice and DSS-fed NLRP3 KO mice. C. Representative images of two-dimensional images 100 μm below the cortical surface at 5min, 15min, 30min, 45min and 60min after infusion of FITC-dextran in cisterna magna (25× water immersion objective). B. Linear and histogram analysis of the FITC-detran intensity in the paravascular space at different time points among control WT, DSS-fed WT, control NLRP3 KO mice and DSS-fed NLRP3 KO mice.

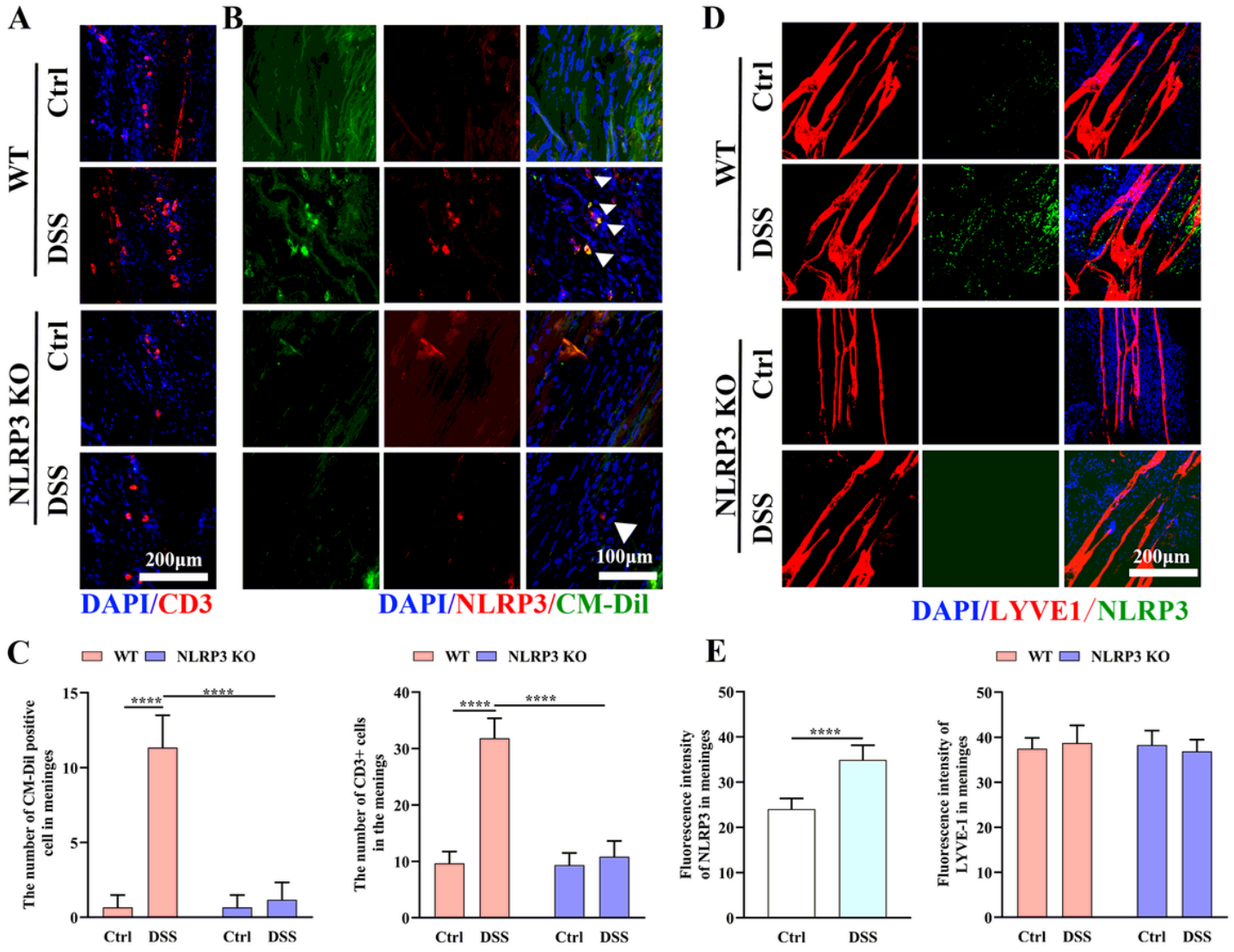

Figure 8

Colitis increased NLRP3 inflammasome expression and accumulation of gut-derived cells in meninges of WT mice but not NLRP3 KO mice. A. Representative images of CD3 immunoexpression in meninges (25× water immersion objective). B. Representative images of CM-Dil-positive (gut-derived) cells and NLRP3 expression in meninges (25× water immersion objective, magnified 3×). C. Comparison of CD3-positive cell number and CM-Dil-positive cell number in meninges of WT and NLRP3 KO mice. D. Representative images of NLRP3 inflammasome and LYVE1 immunoexpression in meninges (25× water immersion objective). E. Comparison of NLRP3 inflammasome and LYVE1 intensities in meninges of WT and NLRP3 KO mice.